Journal of Computational and Applied Mathematics 290 (2015) 553–566

Contents lists available at ScienceDirect

Journal of Computational and Applied Mathematics

journal homepage: www.elsevier.com/locate/cam

An efficient nonconvex regularization for wavelet frame and total variation based image restoration☆

Xiao-Guang Lv [a,b,*], Yong-Zhong Song [a], Fang Li [c]

[a] School of Mathematical Sciences, Nanjing Normal University, Nanjing, Jiangsu, 210097, PR China
[b] School of Science, Huaihai Institute of Technology, Lianyungang, Jiangsu, 222005, PR China
[c] Department of Mathematics, East China Normal University, Shanghai, 200241, PR China

ARTICLE INFO

Article history:
Received 24 May 2015
Received in revised form 6 June 2015

Keywords:
Image restoration
Nonconvex
Wavelet tight frame
Total variation
Firm thresholding

ABSTRACT

In order to improve the quality of the image, many works impose explicit priors on the solution to regularize the ill-posed inverse problem. In this paper, we propose a hybrid variational model which takes advantages of the wavelet tight frame model and the total variation model for image restoration. The core of the method is a new, nonconvex penalty function that is designed for efficient minimization by means of the firm thresholding and soft shrinkage operations. We address the proposed optimization problem by converting it to a constrained problem with variable splitting and using the alternating direction method of multipliers. Numerical examples for image restoration are given to show that the proposed method outperforms some existing methods in terms of the peak signal-to-noise ratio and structural similarity index.

1. Introduction

Due to environmental effects and imperfections in the imaging system, the recorded images are usually degraded by blurring and noise. The goal of image restoration is to recover approximate images of original images from blurred and noisy measurements. The problem of restoration of digital images plays an important role both in daily life applications such as satellite television, magnetic resonance imaging, computer tomography as well as in areas of research and technology such as optics, geographical information systems, microscopy, astronomy, film restoration, and image and video coding [1–4].

Typically, the image formation process is modeled as the following large scale linear system:

$$g = Hf + \eta, \tag{1}$$

where $f \in \mathbb{R}^{n^2}$ represents the true image to be restored, $\eta \in \mathbb{R}^{n^2}$ represents the additive noise, and $g \in \mathbb{R}^{n^2}$ represents the observed, degraded image. In image deblurring, $H \in \mathbb{R}^{n^2 \times n^2}$ related to the spread point function and the boundary condition is an ill-conditioned matrix that models the blurring operation. In image denoising, H is the identity operator.

Three aspects of the image restoration problem make it computationally challenging [5]: the problem is large scale; the noise η is random and only its statistical properties may be known; H is severely ill-conditioned in image deblurring. Over the past decades, many computational methods for the restoration of images have been sought by several researchers.

☆ This research is supported by NSFC (61401172), 973 Program (2011CB707104), Natural Science Foundation of Jiangsu Province (BK20131209), Postdoctoral Research Funds (2013M540454, 1301064B).

* Corresponding author at: School of Mathematical Sciences, Nanjing Normal University, Nanjing, Jiangsu, 210097, PR China.
E-mail addresses: xiaoguanglv@126.com, xiaoguanglv@hhit.edu.cn (X.-G. Lv), yzsong@njnu.edu.cn (Y.-Z. Song), fli@math.ecnu.edu.cn (F. Li).

http://dx.doi.org/10.1016/j.cam.2015.06.006
0377-0427/

A general approach to compute a useful approximation solution of (1) is to replace the system by a better-conditioned nearby system. This replacement is known as the regularization. Usually, regularization methods formulate the image restoration problem as a minimization problem of the form

$$\mathcal{J}(f) = \mathcal{J}_0(f) + \gamma \mathcal{J}_R(f), \tag{2}$$

where the regularization function $\mathcal{J}_R(f)$ is a prior information about the object to be recovered and $\gamma > 0$ is the regularization parameter that controls the balance between the fidelity term $\mathcal{J}_0(f) = \frac{1}{2}\|Hf - g\|_2^2$ and the regularization term $\mathcal{J}_R(f)$. In general, the choice of the regularization function $\mathcal{J}_R(f)$ is related to the features of the images to be restored.

How to choose an effective functional $\mathcal{J}_R(f)$ is an active area of research in the imaging science and its applications. Probably one of the most popular regularization methods is Tikhonov regularization [6]. The regularization functionals used more often are quadratic functionals of the form $R(f) = \|Lf\|_2^2$, where L is usually chosen to be the identity operator or differentiation operator. The Tikhonov regularization method is suitable and effective when the image to be restored is made by diffused objects, such as astronomical images of nebula or certain images from microscopy [7]. Although Tikhonov regularization has the advantage of simple calculations, it produces a smoothing effect on the restored image, i.e., it overly smooths edges which are important features in human perception. To overcome this shortcoming, Rudin, Osher and Fatemi [8] proposed a total variation (TV) based regularization technique, which has the capability of preserving the edge information in the restored image. In the case of TV regularization, the estimated solution is computed by minimizing the objective function $\mathcal{J}(f) = \mathcal{J}_0(f) + \gamma\|Df\|_1$ where D is the discrete gradient operator. The TV regularization is widely used in the denoising of medical images, such as tomographic images and digital radiographies, or photographic images with high frequencies contents [9]. It is shown that total variation methods can realize significantly sharper edges and overall more visually pleasing images, however, on the other hand tend to create piecewise-constant images even in regions with smooth transitions of gray or color values in the original image. The undesired artifact is usually called staircase effect. Staircase solutions fail to satisfy the evaluation of visual quality and they can develop false edges that do not exist in the true image [10,11]. To remedy the drawbacks of classic TV, some other regularization methods such as high-order TV, overlapping TV and hybrid TV are proposed [12–15].

In recent years, sparsity-based priors of images in certain domains have been widely used in many image restoration tasks, which is based on the observation that images usually have sparse representations in some transformed domains such as Fourier transforms, cosine transforms, wavelet or framelet transforms. In order to make use of the sparsity, one solves the image restoration problem (1) in the corresponding transformed domain and finds a sparse solution of (1) in this transformed domain [16]. There are three types of sparsity priors: analysis-based sparsity prior; synthesis-based sparsity prior and balanced sparsity prior [17]. It should be noted that in the case of non-redundant tight frame systems, the models involving the first two sparsity priors behave equally. The balanced sparsity prior model unifies both popular sparse approximation models and provides balanced image quality between sparseness and regularity. For the balanced approach, one can consider it as an intermediate between two above common sparse approximation approaches.

In [18], Cai et al. used the split Bregman iterations to solve minimization problems arising from the analysis-based prior for image restoration and presented a set of new frame based image restoration algorithms that cover several topics in image restorations such as image denoising, deblurring, inpainting, and cartoon-texture image decomposition. In [19], the iterative algorithms based on decoupling of deblurring and denoising steps were proposed for image restoration. In the denoising step, Wen et al. applied the analysis-based prior and used the wavelet shrinkage for the solution. In [20], a synthesis-based method for image deblurring in tight frame domains was proposed. The authors used a modified version of the linearized Bregman iteration for the solution. Motivated by the recent tight frame based methods on image restoration in either the image or the transform domain, the authors in [21] proposed an iterative tight frame algorithm for image inpainting. Numerical experiments were given to illustrate the performance of the proposed algorithm based on the balanced sparsity prior. We know that the wavelet frame based methods are a reasonably effective procedure for noise reduction and blur removal when the image of interest possesses a sparse wavelet representation. However, the methods implemented by pure wavelet thresholding also revoke unpleasant artifacts around discontinuities as a result of Gibbs phenomenon.

In order to further improve the quality of the restored images, some nonconvex regularization methods are proposed. In [22], Nikolova et al. pointed out that nonconvex nonsmooth regularization has advantages over convex regularization for offering better possibilities to recover images with neat edges. However, its practical interest used to be limited due to the difficulty of the computational stage which requires a nonconvex nonsmooth minimization. In [23], Nikolova et al. designed a computational method that efficiently handles the nonsmooth nonconvex minimization. Motivated by the observation that nonconvex regularization methods can better recover flat signal regions, the authors in [24] considered the logarithmic penalty and the arctangent penalty for signal denoising. In their approach, they restrict the nonconvex penalties so as to ensure the strict convexity of the object function. So, the minimizer is unique and can be reliably obtained through convex optimization methods. For nonconvex regularization methods and their applications, we refer the reader to [25–27] and references therein for more details.

In this paper, in order to combine the advantages of the wavelet tight frame based method and the total variation based method and avoid their main drawbacks, we propose a new hybrid variation model for image restoration. The proposed method can reduce the staircase effect and remove the Gibbs oscillations in the restored images. Especially, to induce wavelet-domain sparsity, we apply a nonconvex penalty due to its strong sparsity-inducing properties. We know that the nonconvex regularizer can promote sparsity more strongly, but generally lead to a nonconvex optimization problem

with non-optimal local minimizer. In this paper, we use firm thresholding, a continuous piecewise-linear approximation of hard thresholding, to compute the minimization involving the non-convex penalty. It is known that the firm thresholding is continuous and does not shrink large entries, as desired, it may be of interest, in comparing soft shrinkage and hard thresholding. For the TV term, we employ the classic soft shrinkage operation to compute the corresponding solution.

This paper is outlined as follows. In the next section, we first give some necessary notations and definitions. Then we present the new hybrid model for image restoration and discuss the property of its convexity. In Section 3, we employ the alternating direction method of multipliers (ADMM) to find the solution of the proposed model and analyze the convergence of the implemented algorithm. Some numerical experiments are given in Section 4 to illustrate the performance of the proposed algorithm. We give concluding remarks in Section 5.

2. The proposed model

Before introducing the new model, we give some necessary notations and definitions. Let $W = [W_0^T, W_{1,1}^T, \ldots, W_{1,J}^T, \ldots, W_{Q,1}^T, W_{Q,J}^T]^T \in \mathbb{R}^{(JQ+1)n^2 \times n^2}$ be a multi-level wavelet tight frame transform operator (i.e $W^TW = I$) that converts an image to its wavelet coefficients, in which Q indicates the level of wavelet decomposition and J is the number of high-pass filters that the wavelet system used. So Wf is a multi-level wavelet tight frame transform of f. Let $D = (D^{(1)}; D^{(2)}) \in \mathbb{R}^{2n^2 \times n^2}$ be the discrete gradient operator where $D^{(1)}$ and $D^{(2)}$ be the first-order finite difference matrices in the horizontal and vertical directions, respectively [28]. More precisely, we have $D^{(1)} = I \bigotimes \nabla$ and $D^{(2)} = \nabla \bigotimes I$ where $\nabla = \text{circ}(-1, 1, 0, \ldots, 0)$ is an n-by-n circulant matrix [29].

In this paper, the estimated solution for image restoration is obtained by minimizing the objective function

$$\mathcal{J}(f) = \mathcal{J}_0(f) + \alpha\Phi(Wf) + \beta\Psi(Df) \tag{3}$$

where $\Phi(Wf) = \sum_{i=1}^{(JQ+1)n^2} \phi((Wf)_i)$ and $\Psi(Df) = \sum_{i=1}^{n^2} \psi((Df)_i)$ with

$$\phi(x) = \begin{cases} |x| - \dfrac{x^2}{2\mu}, & \text{if } |x| < \mu, \\ \dfrac{\mu}{2}, & \text{if } |x| \geq \mu \end{cases}$$

and

$$\psi(x) = |x|, \quad x \in \mathbb{R}.$$

In the function ϕ, $\mu > 0$ is a firm thresholding parameter. See [30] for more details. It is not difficult to see that ϕ is a nonconvex function. In this paper, we use the nonconvex term $\Phi(Wf)$ to improve the wavelet-domain sparsity of the restored images. Recently, many nonconvex functions such as the logarithmic penalty, the arctangent penalty, the first-order rational function and the l_p function ($0 < p < 1$) are proposed for image restoration; see [23,24,26] for more details. In [26], Woodworth and Chartrand demonstrated that compared with other nonconvex functions, the penalty function induced by firm thresholding can be better for recovering sparse signals and images. More precisely, we plot the widely used nonconvex functions in Fig. 1. From Fig. 1, it is not difficult to see that the firm thresholding inducing penalty function can promote sparsity better.

In the following, we discuss the convexity of the objective function. Assume that $\Lambda = \text{diag}(\Lambda_1, \ldots, \Lambda_{n^2})$ is a diagonal matrix where $\Lambda_i = 1$ if $|(Wf)_i| < \mu$ and $\Lambda_i = 0$ if $|(Wf)_i| \geq \mu$. Hence we can rewrite the proposed objective function as follows:

$$\mathcal{J}(f) = \frac{1}{2}\|Hf - g\|_2^2 + \alpha\|\Lambda Wf\|_1 - \frac{\alpha}{2\mu}\|\Lambda Wf\|_2^2 + \frac{\alpha\mu}{2}\|(I - \Lambda)e\|_1 + \beta\|Df\|_1 \tag{4}$$

where e is a vector with all entries equal to 1, i.e., $e = (1, \ldots, 1)^T$. For the convexity of the objective function, we have the following theorem.

Theorem 1. *If $H^TH - \frac{\alpha}{\mu}W^T\Lambda W$ is positive definite, then the objective function $\mathcal{J}(f)$ proposed in (3) is strictly convex.*

Proof. The function $\mathcal{J}(f)$ can be rewritten as

$$\mathcal{J}(f) = \Theta_1(f) + \Theta_2(f) + \Theta_3(f) \tag{5}$$

where

$$\Theta_1(f) = \frac{1}{2}\|Hf - g\|_2^2 - \frac{\alpha}{2\mu}\|Wf\|_2^2,$$
$$\Theta_2(f) = \alpha\|\Lambda Wf\|_1 - \frac{\alpha}{2\mu}\|(I - \Lambda)Wf\|_2^2 + \frac{\alpha\mu}{2}\|(I - \Lambda)e\|_1,$$
$$\Theta_3(f) = \beta\|Df\|_1.$$

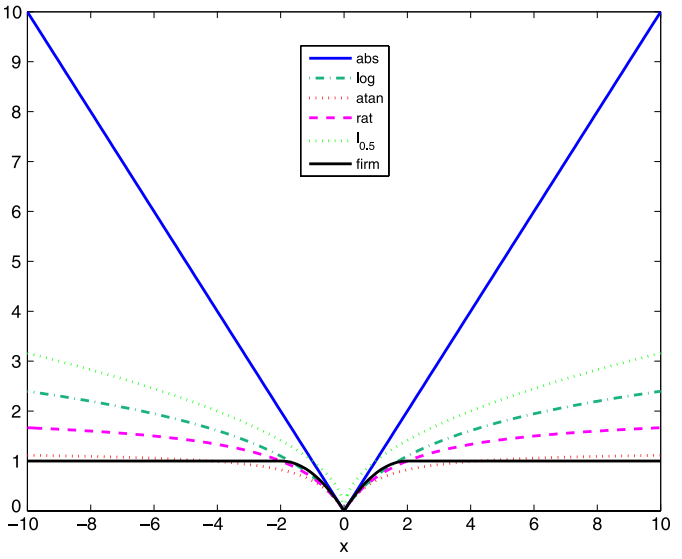

Fig. 1. Nonconvex penalty functions.

It is obvious that the function $\Theta_3(f)$ is convex. If $H^TH - \frac{\alpha}{\mu}W^T\Lambda W$ is positive definite, the function $\Theta_1(f)$ is strictly convex. In the following, we discuss the convexity of the function $\Theta_2(f)$.

Define the function $\varphi(x)$ as the following form

$$\varphi(x) = \phi(x) + \frac{x^2}{2u} = \begin{cases} |x|, & \text{if } |x| < \mu, \\ \dfrac{\mu}{2} + \dfrac{x^2}{2\mu}, & \text{if } |x| \geq \mu. \end{cases}$$

Now we discuss $\varphi(x)$ as follows.

Case 1: If $0 < x < \mu$, then $\varphi(x) = x$. We have that $\varphi'(x) = 1$ and $\varphi''(x) = 0$.

Case 2: If $-\mu < x < 0$, then $\varphi(x) = -x$. We have that $\varphi'(x) = -1$ and $\varphi''(x) = 0$.

Case 3: If $|x| > \mu$, then $\varphi(x) = \frac{\mu}{2} + \frac{x^2}{2\mu}$. We have that $\varphi'(x) = \frac{x}{\mu}$ and $\varphi''(x) = \frac{1}{\mu}$.

By the definition of $\varphi(x)$, we know that it is twice differentiable on $\mathbb{R}/\{-\mu, 0, \mu\}$; With the discussion of $\varphi(x)$, we have $\varphi'_-(-\mu) = \varphi'_+(-\mu)$, $\varphi'_-(0) < \varphi'_+(0)$ and $\varphi'_-(\mu) = \varphi'_+(\mu)$. By Theorem 6.4 of [31], we have that a function is convex if it has an increasing right-derivative. Therefore, $\varphi(x)$ is a convex function.

We rewrite the function $\Theta_2(f)$ as a sum of the form

$$\Theta_2(f) = \sum_{i=1}^{(JQ+1)n^2} \varphi((Wf)_i)$$

with

$$\varphi((Wf)_i) = \begin{cases} |(Wf)_i|, & \text{if } |(Wf)_i| < \mu, \\ \dfrac{\mu}{2} + \dfrac{(Wf)_i^2}{2\mu}, & \text{if } |(Wf)_i| \geq \mu. \end{cases}$$

Since the linear transformation can keep the convexity of the function $\varphi(\cdot)$, we get that the function $\Theta_2(f)$ is convex.

From the above discussions, the objective function $\mathcal{J}(f)$ is a sum of two convex functions and one strictly convex function when $H^TH - \frac{\alpha}{\mu}W^T\Lambda W$ is positive definite. Therefore, we get that $\mathcal{J}(f)$ is strictly convex if the matrix $H^TH - \frac{\alpha}{\mu}W^T\Lambda W$ is positive definite. □

For image denoising, we have $H = I$. In this case, $\mathcal{J}(f)$ is strictly convex if $\mu > \alpha$. Note that α is a regularization parameter which is small enough in practice. On the other hand, μ is bigger than α, since it is a thresholding of $|(Wf)_i|$. Therefore, the objective function $\mathcal{J}(f)$ is always strictly convex for image denoising. For image deblurring, H is an ill-conditioned matrix, so we need a larger μ and a smaller α such that $\mathcal{J}(f)$ is strictly convex. The existence and uniqueness of the solution of (3) are guaranteed by the convexity of $\mathcal{J}(f)$.

3. Optimization algorithm

We recall the variable splitting method for solving separable convex optimization problems with linear constraints. Consider the following convex optimization problem:

$$\begin{aligned} &\min && \theta_1(x_1) + \theta_2(x_2) \\ &\text{subject to} && A_1x_1 + A_2x_2 = b, \\ &&& x_i \in \mathcal{X}_i,\ i = 1, 2 \end{aligned} \tag{6}$$

where $\theta_i : \mathcal{X}_i \to \mathbb{R}$ are closed convex functions, $A_i \in \mathbb{R}^{l\times m_i}$ are linear transforms and $b \in \mathbb{R}^l$ is a given vector. If it has an optimal solution $(x_1^*, x_2^*) \in \mathcal{X}_1 \times \mathcal{X}_2$, then its dual problem also has an optimal solution $\lambda^* \in \mathbb{R}^l$, since the problem (6) is a convex programming problem with linear constraints. The task of solving the problem (6) is to find $(x_1^*, x_2^*, \lambda^*) \in \mathcal{X}_1 \times \mathcal{X}_2 \times \mathbb{R}^l$, such that

$$\begin{cases} \theta_1(x_1) - \theta_1(x_1^*) + (x_1 - x_1^*)^T(-A_1^T\lambda^*) \geq 0, \\ \theta_2(x_2) - \theta_2(x_2^*) + (x_2 - x_2^*)^T(-A_2^T\lambda^*) \geq 0, \quad \forall (x_1, x_2, \lambda) \in \mathcal{X}_1 \times \mathcal{X}_2 \times \mathbb{R}^l. \\ (\lambda - \lambda^*)^T(A_1x_1^* + A_2x_2^* - b) \geq 0. \end{cases} \tag{7}$$

Usually, the augmented Lagrangian method is used to find the solution $(x_1^*, x_2^*, \lambda^*)$. It is known that the augmented Lagrangian function of optimization problem in (6) is defined as

$$\mathcal{L}(x_1, x_2, \lambda) = \theta_1(x_1) + \theta_2(x_2) - \lambda^T(A_1x_1 + A_2x_2 - b) + \frac{\sigma}{2}\|A_1x_1 + A_2x_2 - b\|^2 \tag{8}$$

where $\lambda \in \mathbb{R}^l$ is the Lagrange multiplier and σ is a penalty parameter, which controls the linear constraint [32]. The idea of the ADMM is to iteratively solve the following subproblems:

$$\begin{cases} x_1^{k+1} = \arg\min\limits_{x_1\in\mathcal{X}_1} \mathcal{L}(x_1, x_2^k, \lambda^k), \\ x_2^{k+1} = \arg\min\limits_{x_2\in\mathcal{X}_2} \mathcal{L}(x_1^{k+1}, x_2, \lambda^k), \\ \lambda^{k+1} = \lambda^k - \sigma(A_1x_1^{k+1} + A_2x_2^{k+1} - b). \end{cases} \tag{9}$$

The main advantage of the ADMM is to make full use of the separable structure of the objective function $\theta_1(x_1) + \theta_2(x_2)$. The ADMM (9) is a splitting version of the augmented Lagrangian method where the augmented Lagrangian method's subproblem is decomposed into two subproblems in the Gauss–Seidel fashion at each iteration, and thus the variables x_1 and x_2 can be solved separably in the alternating order [33,34].

Notice that the terms added to $\theta_1(x_1) + \theta_2(x_2)$ in the definition of the augmented Lagrangian function $\mathcal{L}(x_1, x_2, \lambda)$ in (8) can be written as a single quadratic term, leading to the following alternative form of (9):

$$\begin{cases} x_1^{k+1} = \arg\min\limits_{x_1\in\mathcal{X}_1} \theta_1(x_1) + \dfrac{\sigma}{2}\|A_1x_1 + A_2x_2^k - b + d^k\|_2^2, \\ x_2^{k+1} = \arg\min\limits_{x_2\in\mathcal{X}_2} \theta_2(x_2) + \dfrac{\sigma}{2}\|A_1x_1^{k+1} + A_2x_2 - b + d^k\|_2^2, \\ d^{k+1} = d^k + (A_1x_1^{k+1} + A_2x_2^{k+1} - b). \end{cases} \tag{10}$$

It is easy to see that $e^k = -\frac{\lambda^k}{\sigma}$ where λ^k is determined by (9). In this case, we derive the following ADMM algorithm:

Algorithm 1 ADMM for the minimization problem (6)

initialization: Starting point (x_1^0, x_2^0, e^0), $\sigma > 0$,
iteration:
$x_1^{k+1} = \arg\min_{x_1} \theta_1(x_1) + \frac{\sigma}{2}\|A_1x_1 + A_2x_2^k - b + d^k\|_2^2$;
$x_2^{k+1} = \arg\min_{x_2} \theta_2(x_2) + \frac{\sigma}{2}\|A_1x_1^k + A_2x_2 - b + d^k\|_2^2$;
$d^{k+1} = d^k + (A_1x_1^{k+1} + A_2x_2^{k+1} - b)$;
$k = k + 1$;
until a stopping criterion is satisfied.

In the following, we discuss the implementation details of the ADMM algorithm to the proposed model in (3). By introducing new auxiliary variables u, v, the problem (3) can be reformulated as the following constrained optimization problem:

$$\begin{aligned} &\min_{f,u,v} && \frac{1}{2}\|Hf - g\|_2^2 + \alpha\Phi(u) + \beta\Psi(v). \\ &s.t. && Wf = u, Df = v. \end{aligned} \tag{11}$$

It is not difficult to see that the problem (11) is a special case of problem in (6) with the following specifications:

$$A_1 = \begin{pmatrix} W \\ D \end{pmatrix}, \qquad A_2 = \begin{pmatrix} -I & 0 \\ 0 & -I \end{pmatrix}, \qquad x_1 = f, \qquad x_2 = \begin{pmatrix} u \\ v \end{pmatrix}, \qquad d = \begin{pmatrix} 0 \\ 0 \end{pmatrix}.$$

We are going to use Algorithm 1 for solving the proposed model, so we specify the augmented Lagrangian function of (3) as the following form:

$$\mathcal{L}(f, u, v, d_1, d_2) = \frac{1}{2}\|Hf - g\|_2^2 + \alpha\Phi(u) + \frac{\sigma_1}{2}\|Wf - u + d_1\|_2^2 + \beta\Psi(v) + \frac{\sigma_2}{2}\|Df - v + d_2\|_2^2. \tag{12}$$

To minimize $\mathcal{L}$ with respect to f, we solve the subproblem

$$\min_f \frac{1}{2}\|Hf - g\|_2^2 + \frac{\sigma_1}{2}\|Wf - u^k + d_1^k\|_2^2 + \frac{\sigma_2}{2}\|Df - v^k + d_2^k\|_2^2. \tag{13}$$

The minimizer can be obtained by equivalently solving a linear system

$$(H^TH + \sigma_1 W^TW + \sigma_2 D^TD)f = H^Tg + \sigma_1 W^T(u^k - d_1^k) + \sigma_2(v^k - d_2^k). \tag{14}$$

Note that $W^TW = I$ and H, D have block circulant with circulant blocks (BCCB) structure when periodic boundary conditions are used [28,35,36]. We know that the computations with BCCB matrices can be very efficient by using fast Fourier transforms (FFTs).

To minimize $\mathcal{L}$ over u, we solve

$$\min_u \frac{\alpha}{\sigma_1}\Phi(u) + \frac{1}{2}\|u - (Wf^{k+1} + d_1^k)\|_2^2 = \sum_{i=1}^{(JQ+1)n^2} \frac{\alpha}{\sigma_1}\phi(u_i) + \frac{1}{2}\|u - (Wf^{k+1} + d_1^k)\|_2^2 \tag{15}$$

where

$$\phi(x) = \begin{cases} |x| - \dfrac{x^2}{2\mu}, & \text{if } |x| < \mu, \\ \dfrac{\mu}{2}, & \text{if } |x| \geq \mu. \end{cases}$$

Note that the minimization in (15) is separable. With respect to each component, it is easy to show that the solution of (15) is

$$u_i^{k+1} = s_{\text{firm}}\left((Wf^{k+1} + d_1^k)_i, \frac{\alpha}{\sigma_1}, \mu\right) \tag{16}$$

where

$$s_{\text{firm}}(x, \delta, \mu) = \begin{cases} 0, & \text{if } |x| < \delta, \\ \dfrac{\mu}{\mu - \delta}(x - \delta\,\text{sign}(x)), & \text{if } \delta \leq |x| \leq \mu, \\ x, & \text{if } |x| > \mu. \end{cases}$$

It is shown that firm thresholding has a phase transition threshold that is strictly better than that of soft shrinkage.

As for the sub-problem with respect to v, we have

$$\min_v \frac{\beta}{\sigma_2}\Psi(v) + \frac{1}{2}\|v - (Df^{k+1} + d_2^k)\|_2^2 = \sum_{i=1}^{2n^2} \frac{\beta}{\sigma_2}\psi(v_i) + \frac{1}{2}\|v - (Df^{k+1} + d_2^k)\|_2^2 \tag{17}$$

where $\psi(x) = |x|$. This minimization can be solved explicitly by the soft shrinkage operator:

$$v_i^{k+1} = s_{\text{soft}}\left((Df^{k+1} + d_2^k)_i, \frac{\beta}{\sigma_2}\right) \tag{18}$$

where

$$s_{\text{soft}}(x, \delta) = \begin{cases} 0, & \text{if } |x| < \delta, \\ x - \delta\,\text{sign}(x), & \text{if } |x| \geq \delta. \end{cases}$$

On the other hand, the updating scheme of the Lagrangian multipliers can be rewritten specifically as

$$\begin{aligned} d_1^{k+1} &= d_1^k + Wf^{k+1} - u^{k+1}, \\ d_2^{k+1} &= d_2^k + Df^{k+1} - v^{k+1}. \end{aligned} \tag{19}$$

To sum up, we obtain the following algorithm for the image restoration problem.

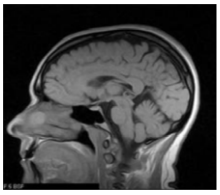
(a) Brain.


(b) House.


(c) Bridge.


(d) Barbara.

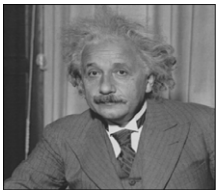
(e) Einstein.


(f) Elaine.


(g) Zelda.


(h) Car.


(i) Butterfly.

Fig. 2. Original images.

Algorithm 2 ADMM for the image restoration problem (3)

initialization: $u = g$, $v = g$, $k = 0$, α, β, μ, H, σ_i and $d_i^0 = 0$ for $i = 1, 2$.
iteration:
a. Compute f^{k+1} by solving (14) with the fast algorithm;
b. Compute u^{k+1} by using the firm thresholding (16);
c. Compute v^{k+1} by using the soft shrinkage (18);
e. Update d_i^{k+1} for $i = 1, 2$ according to (19);
g. $k = k + 1$;
until a stopping criterion is satisfied.

There are many convergence results for ADMM discussed in the literature. For convex functions $\theta_1(x_1)$ and $\theta_2(x_2)$ the sequence generated by ADMM converges even if each subproblem is not solved exactly [37]. To be more specific, this algorithm converges to a solution of the objective function if the errors are summable. We refer the reader to [38–40] for the convergences of ADMM and its variant in detail. Note that for our problem, $\theta_2(x_2) = \alpha\Phi(u) + \beta\Psi(v)$ is not convex even if the objective function $\mathcal{J}(f)$ proposed in (3) is strictly convex. However, all our experiments show that Algorithm 2 converges to the unique global minimizer since the objective function is strictly convex and all minimization subproblems are solved exactly.

4. Numerical examples

In this section, we give some numerical experiments for comparing the proposed hybrid model with other state-of-the-art methods such as tight frame model (Frame) and total variation model (TV) for image restoration. The tight frame model for image restoration in [18] is solved by the alternating split Bregman algorithm. It is noted in [41] that the alternating split Bregman algorithm is equivalent to the ADMM algorithm. The total variation model for image restoration is solved by some efficient methods such as the alternating minimization algorithm [28], primal–dual method, the alternating split Bregman algorithm and the ADMM algorithm [35]. In this paper, we employ the ADMM algorithm to solve the tight frame model and the standard total variation model for a fair comparison. All computations of the present paper were carried out in Matlab R2013b. The results were obtained by running the Matlab codes on an Intel(R) Core(TM) i5-4200 CPU (1.60 GHz, 2.30 GHz) computer with RAM of 4 GB.

To measure the quality of the restored images, we use the peak signal-to-noise ratio (PSNR) and Structural SIMilarity index (SSIM) defined as follows:

$$\mathrm{PSNR} = 10\log_{10}\left(\frac{255^2 n^2}{\|\hat{f} - f\|_2^2}\right)$$

and

$$\mathrm{SSIM} = \frac{(2\mu_f\mu_{\hat{f}} + C_1)(2\sigma_{f\hat{f}} + C_2)}{(\mu_f^2 + \mu_{\hat{f}}^2 + C_1)(\sigma_f^2 + \sigma_{\hat{f}}^2 + C_2)}$$

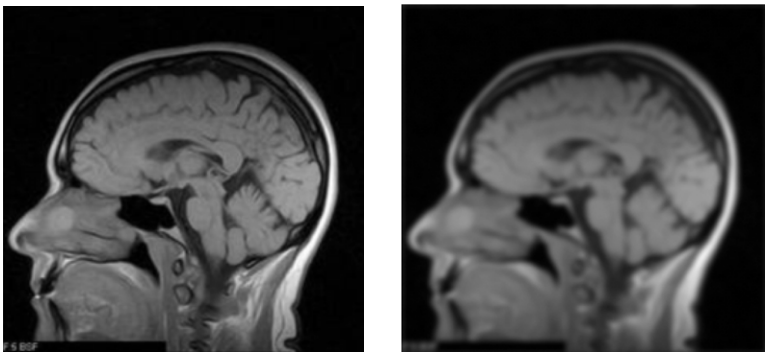

(a) True. (b) Degraded.

(c) Frame. (d) TV. (e) Proposed.

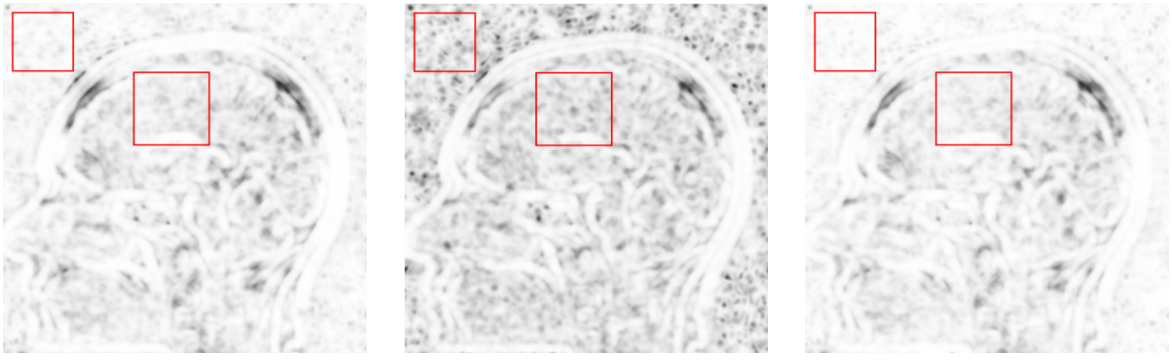

(f) Frame. (g) TV. (h) Proposed.

Fig. 3. Restoration results for the image "Brain" under the out-of-focus blur and the noise with BSNR = 40 ($\alpha = \beta = 0.005$, $\mu = 5\alpha/\sigma_1$).

where f and $\hat{f}$ are the ideal image and the restored image with size of $n \times n$, respectively. μ_f and $\mu_{\hat{f}}$ are averages of u and $\hat{u}$ respectively, σ_f and $\sigma_{\hat{f}}$ are the variances of u and $\hat{f}$ respectively and $\sigma_{f\hat{f}}$ is the covariance of f and $\hat{f}$. The positive constants C_1 and C_2 can be thought of as stabilizing constants for near-zero denominator values [42]. In the following experiments, we will use the SSIM map to reveal areas of high or low similarity between two images. It is noted that the whiter the SSIM map is, the closer between the two images are in structure. The perfect reconstruction would have SSIM value equal to 1.

We use the stopping criterion when the maximum number of allowed outer iterations N has been carried out or the relative differences between consecutive iterates $f^1, f^2, f^3, \ldots$ satisfy

$$\frac{\|f^{k+1} - f^k\|_2}{\|f^{k+1}\|_2} < \varepsilon.$$

In this paper, we set $N = 100$ and $\varepsilon = 10^{-3}$ for the three algorithms. In order to make the results more convincing, we compare these algorithms with different regularization parameters. We use the best regularization parameters such that

(a) True. (b) Degraded.

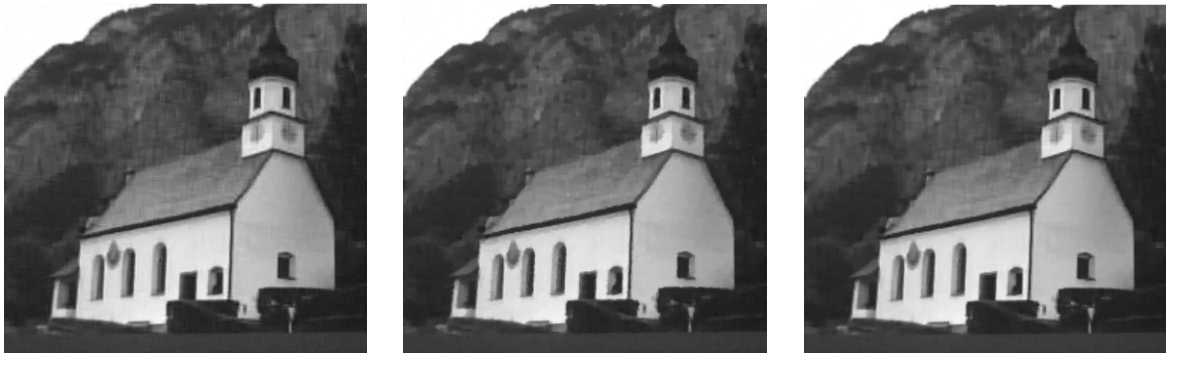

(c) Frame. (d) TV. (e) Proposed.

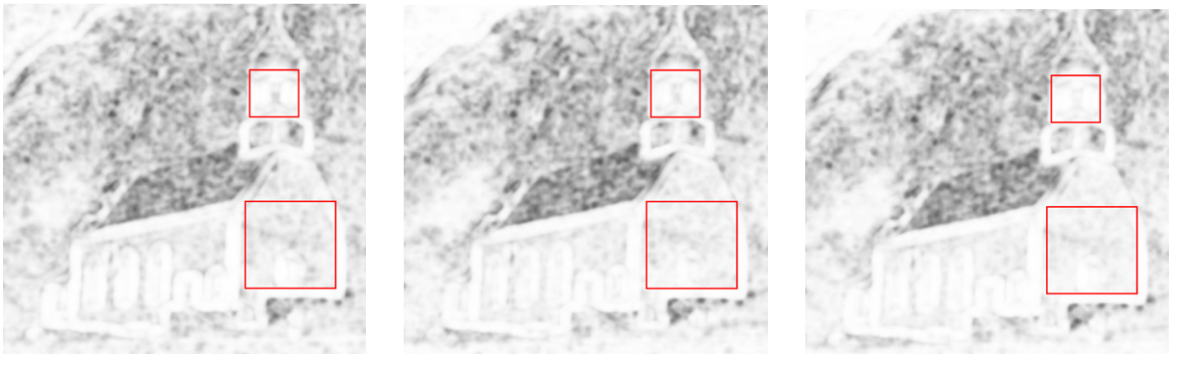

(f) Frame. (g) TV. (h) Proposed.

Fig. 4. Restoration results for the image "House" under the out-of-focus blur and the noise with BSNR = 40 ($\alpha = \beta = 0.006$, $\mu = 3\alpha/\sigma_1$).

the optimal PSNR values are achieved. It should be noted that the ADMM algorithm converges for any choice of the penalty parameter. However, this parameter does influence the speed of the algorithms [43]. In numerical experiments, we set the penalty parameter $\sigma_1 = 0.001$ and $\sigma_2 = 0.001$ empirically.

The test images are shown in Fig. 2. The sizes of the first five images are 256×256 while the sizes of the last four are 512×512. In order to simulate the degraded operation in the tests, we generate the blurred and noisy images by blurring the true images with the given different point spread functions and then adding the noise with different BSNR. The BSNR is given by

$$\mathrm{BSNR} = 10 \log_{10} \frac{\|g\|_2^2}{\|\eta\|_2^2}$$

where g and η are the degraded image and the noise added in the tests, respectively. For each image, we consider three different blurs: the out-of-focus blur proposed in [44], the Gauss blur function *psfGauss* proposed in [45] and the linear

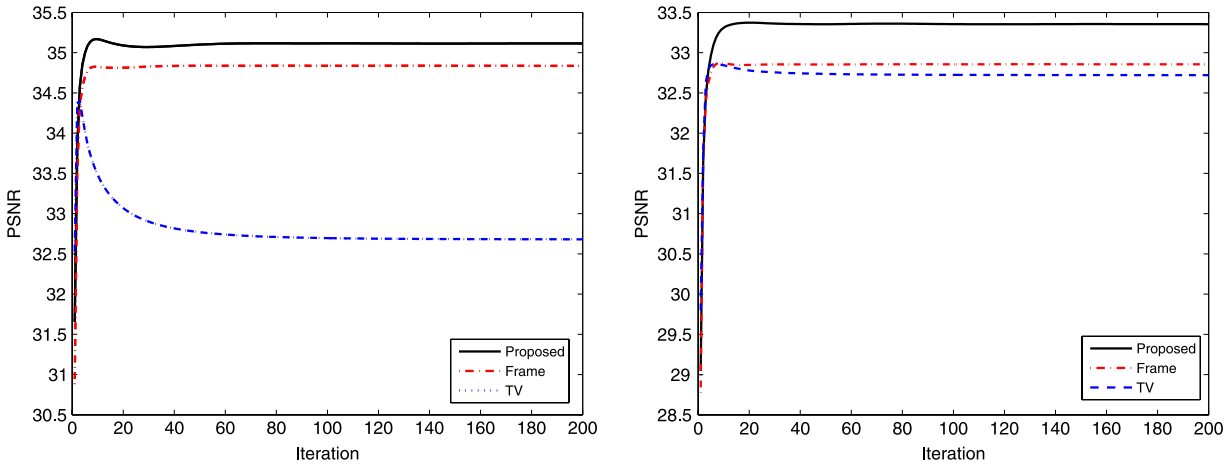

(a) Brain. (b) House.

Fig. 5. Convergence results for the images "Brain" and "House" under the out-of-focus blur and the noise with BSNR = 40.

Table 1
Comparison of the performance of three methods with different blur kernels.

	Blur	BSNR	PSNR			SSIM		
			Frame	TV	Proposed	Frame	TV	Proposed
Brain	Defocus	40	34.81	33.19	**35.11**	0.9347	0.8908	**0.9435**
	Motion	35	37.52	37.23	**38.01**	0.9536	0.9607	**0.9634**
	Gauss	30	33.49	31.44	**33.53**	0.9360	0.9164	**0.9364**
House	Defocus	40	32.85	32.81	**33.41**	0.8725	0.8744	**0.8821**
	Motion	35	35.56	35.64	**36.07**	0.9192	0.9279	**0.9292**
	Gauss	30	31.00	30.42	**31.53**	0.8569	0.8511	**0.8627**
Bridge	Defocus	40	25.27	25.24	**25.34**	0.7784	0.7803	**0.7811**
	Motion	35	29.76	29.88	**30.16**	0.9164	0.9194	**0.9244**
	Gauss	30	23.24	23.14	**23.36**	0.6442	0.6452	**0.6568**
Barbara	Defocus	40	28.99	28.57	**29.06**	0.8577	0.8410	**0.8633**
	Motion	35	32.41	31.90	**32.55**	0.9267	0.9245	**0.9363**
	Gauss	30	25.46	25.16	**25.58**	0.7154	0.7162	**0.7547**
Einstein	Defocus	40	33.31	33.05	**33.48**	0.8662	0.8595	**0.8706**
	Motion	35	36.67	36.40	**36.92**	0.9271	0.9236	**0.9299**
	Gauss	30	30.95	30.92	**31.66**	0.8190	0.8136	**0.8289**
Elaine	Defocus	40	32.74	32.57	**32.79**	0.9596	0.9575	**0.9598**
	Motion	35	35.24	34.91	**35.30**	0.9783	0.9777	**0.9793**
	Gauss	30	32.16	31.82	**32.29**	0.9558	0.9535	**0.9565**
Zelda	Defocus	40	37.05	36.43	**37.25**	0.9789	0.9767	**0.9803**
	Motion	35	38.63	38.41	**38.86**	0.9878	0.9880	**0.9887**
	Gauss	30	35.51	34.82	**35.91**	0.9771	0.9733	**0.9774**
Car	Defocus	40	31.73	31.50	**31.98**	0.9643	0.9597	**0.9677**
	Motion	35	34.42	34.53	**34.84**	0.9798	0.9814	**0.9819**
	Gauss	30	29.73	28.80	**29.79**	0.9533	0.9492	**0.9541**
Butterfly	Defocus	40	32.15	31.97	**32.51**	0.9718	0.9697	**0.9751**
	Motion	35	34.48	33.61	**35.47**	0.9853	0.9772	**0.9875**
	Gauss	30	30.56	30.00	**30.64**	0.9658	0.9621	**0.9663**

motion blur in [46]. In this paper, we choose the out-of-focus blur with radius 9 which is generated by the MATLAB function *ones*(9, 9)/81. It is known that the point spread function for the linear motion blur is represented by a line segment of length r pixels in the direction of the motion. The angle θ (in degrees) specifies the direction and is measured counter-clockwise from the positive x-axis. In this paper, $r = 7$ and $\theta = 45$. Obviously, the Gauss blur *psfGauss*(*dim*, s) is related with the dimension of the point spread function array *dim* and the standard deviation s. In this paper, we choose $dim = 7$ and $s = 2$.

In Figs. 3 and 4, we show the restoration results when the tight frame method, the total variation method and the hybrid method are applied to the image restoration problem for the out-of-focus blur and the noise with BSNR = 40. From the visual quality of restored images, the proposed method is competitive with the other two methods. For showing the effectiveness of our method, we give the SSIM maps of the restored images with respect to the original image in Figs. 3(f)–(h) and 4(f)–(h).

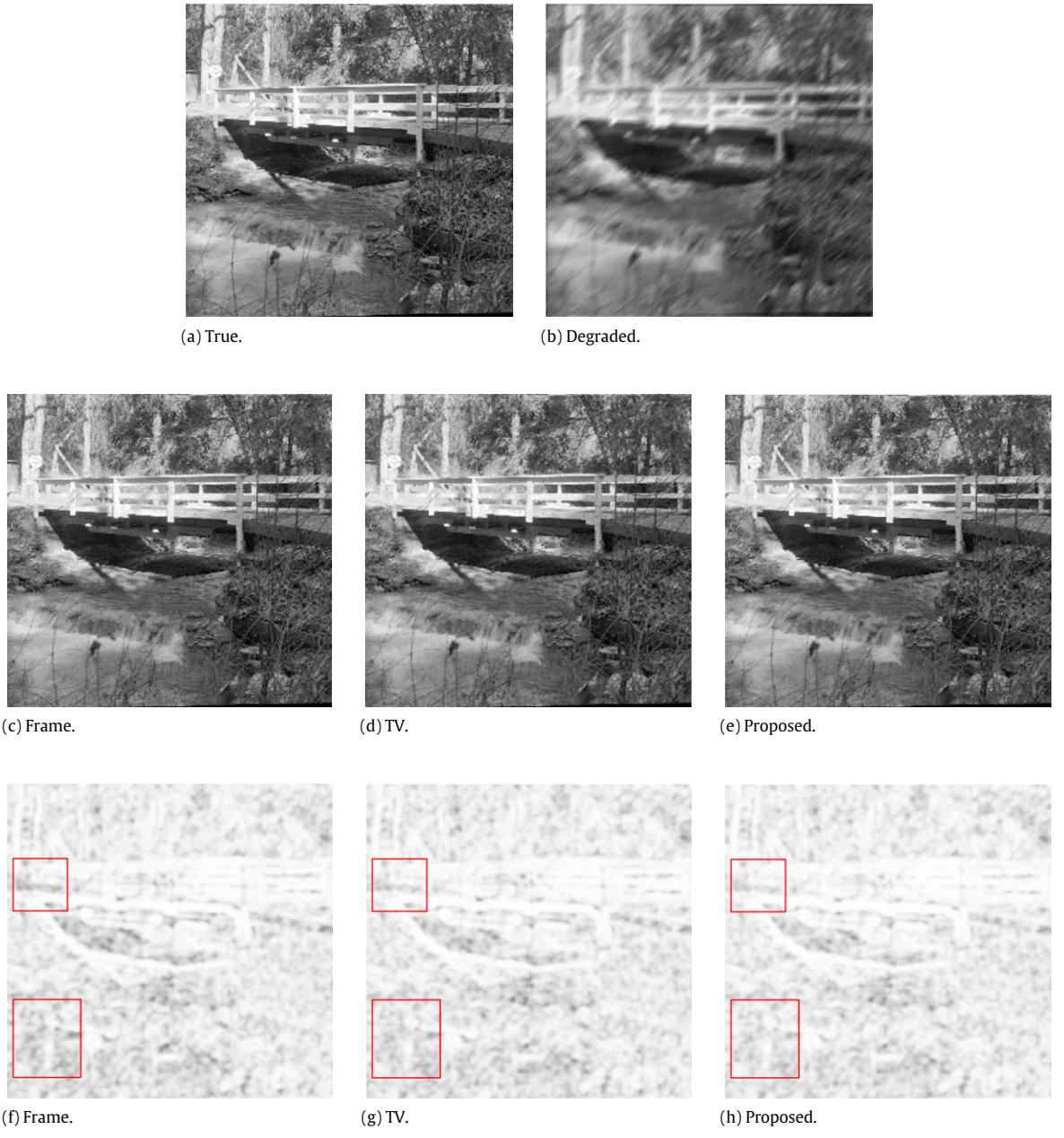

(a) True. (b) Degraded.

(c) Frame. (d) TV. (e) Proposed.

(f) Frame. (g) TV. (h) Proposed.

Fig. 6. Restoration results for the image "Bridge" under the motion blur and the noise with BSNR = 35 ($\alpha = \beta = 0.01$, $\mu = 2\alpha/\sigma_1$).

The SSIM is a well-known quality metric used to measure the similarity between two images. It is based on three specific statistical measures that are much closer to how the human eye perceives differences between images. From these figures, it is not difficult to see that the SSIM maps of our method are slight whiter than the others especially in the marked rectangle regions. The comparison of the PSNR and SSIM values in Table 1 also proves that our method yields a better restoration result. In Fig. 5, we plot the convergence results about PSNR versus iteration for different methods. We observe that the proposed method is convergent and get higher PSNR values than others.

In Fig. 6, we report the experiment on the Bridge image degraded by the motion blur and the noise with BSNR = 35. The original image and the blurred image with noise are shown in Figs. 6(a)–(b). The restored images produced by the tight frame method, the total variation method and the proposed method are shown in Figs. 6(c)–(e). From these figures, we observe that the restored image by our model is much better than other models in terms of the staircase effect, Gibbs artifact and edge preservation. The proposed method performs better, with SSIM values 0.9224 versus 0.9164 and 0.9194 in the tight frame method and the total variation method respectively. From Figs. 6(f)–(h) we also observe that the SSIM map of the

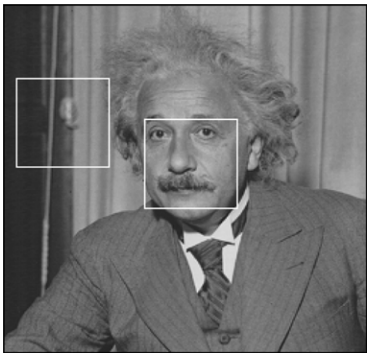

(a) True.

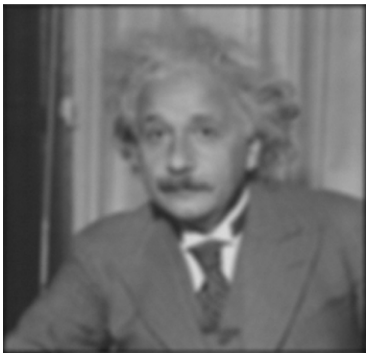

(b) Degraded.

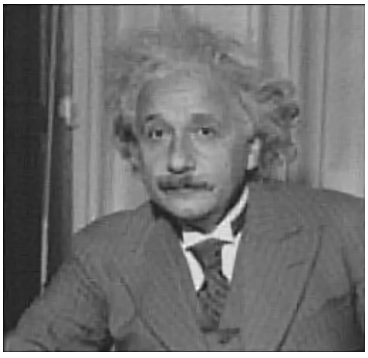

(c) Frame.

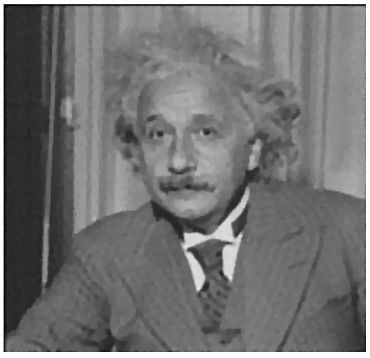

(d) TV.

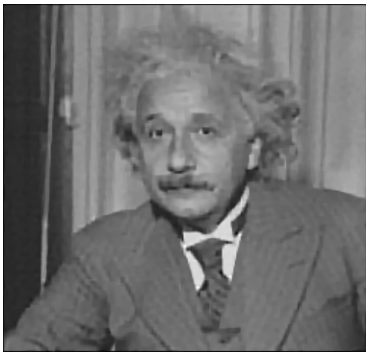

(e) Proposed.

Fig. 7. Restoration results for the image "Einstein" under the Gauss blur and the noise with BSNR = 30 ($\alpha = \beta = 0.01$, $\mu = 2\alpha/\sigma_1$).

restored images by the proposed method is whiter than those by the other two methods. See the marked rectangles for example. Our method can get better SSIM map results. From Table 1, we know that, compared with the other two methods, the proposed method performs better for restoring images with respect to the PSNR and SSIM values,

The third example is the test on the Einstein image. The original image, the degraded image and the restoration images by the tight frame method and the total variation method and the proposed approach are exhibited in Figs. 7(a)–(e). Visually, the proposed method is better than the other two methods since the image recovered by the proposed method preserves more details and looks more natural. One can observe that the Gibbs effect of the tight frame method is rather clear and the result of the TV method is rather clean but some details are lost. Our new approach avoids entirely the Gibbs oscillation and the details are better recovered.

For a better visual comparison, we have enlarged some details of the three restored images in Figs. 8 and 9. As can be seen in the zoomed parts (the part shown as the white rectangle in Fig. 7(a)), our method has less staircase effects and makes a good compromise between edge preserving and smoothing. The result of the tight frame method has visible Gibbs oscillation particularly in those rather flat regions and the total variation method loses some crucial details due to the smoothing effect. It is not difficult to see that the images of Figs. 8(e) and 9(e) look more natural where the Gibbs oscillation has been successfully alleviated and the staircase effect has been reduced.

In Table 1, we report the PSNR and SSIM values for all nine test images in detail. From the table, we see that our method has higher PSNR and SSIM values than the other two methods. Therefore, we conclude that the proposed method performs better than the tight frame method and the total variation method.

5. Conclusions

In this paper, we investigate a nonconvex hybrid variational regularization for restoring the degraded images. The proposed model takes advantage of the wavelet tight frame model and the total variation model. In particular, we apply a nonconvex term to induce wavelet-domain sparsity due to its strong sparsity-inducing properties. We prove that the proposed model is strictly convex and solve the proposed optimization model by using the ADMM method. Various numerical results were reported to exhibit the performance of the new model. It is clear that this model can recover better details than the total variation method and avoid efficiently the Gibbs oscillation of the tight frame method.

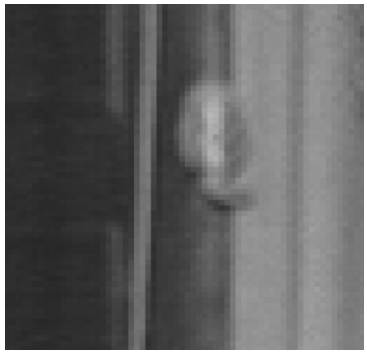

(a) True.

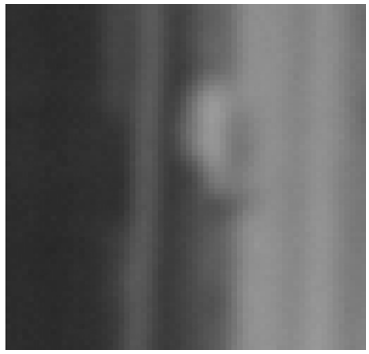

(b) Degraded.

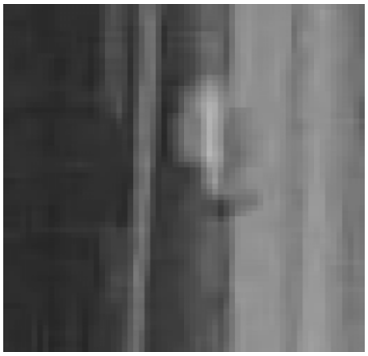

(c) Frame.

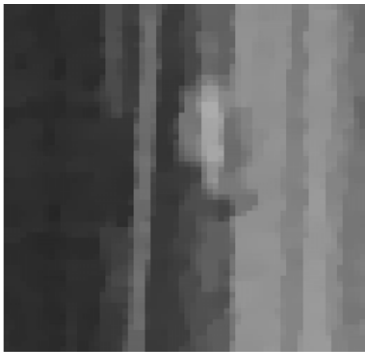

(d) TV.

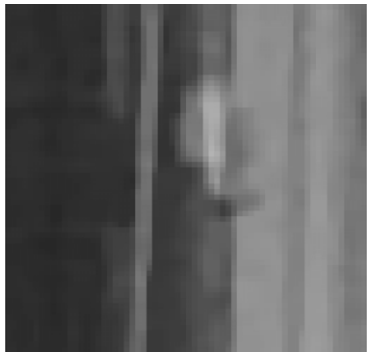

(e) Proposed.

Fig. 8. Comparison of a small portion of the restored images for the image "Einstein" under the Gauss blur and the noise with BSNR = 30.

(a) True.

(b) Degraded.

(c) Frame.

(d) TV.

(e) Proposed.

Fig. 9. Comparison of a small portion of the restored images for the image "Einstein" under the Gauss blur and the noise with BSNR = 30.

References

[1] Mark R. Banham, Aggelos K. Katsaggelos, Digital image restoration, IEEE Signal Process. Mag. 14 (2) (1997) 24–41.
[2] Curtis R. Vogel, Computational Methods for Inverse Problems, Vol. 23, SIAM, 2002.
[3] Tony F. Chan, Jianhong Jackie Shen, Image Processing and Analysis: Variational, PDE, Wavelet, and Stochastic Methods, SIAM, 2005.
[4] Per Christian Hansen, James G. Nagy, Dianne P. O'leary, Deblurring Images: Matrices, Spectra, and Filtering, Vol. 3, SIAM, 2006.
[5] James G. Nagy, Katrina Palmer, Lisa Perrone, Iterative methods for image deblurring: a matlab object-oriented approach, Numer. Algorithms 36 (1) (2004) 73–93.
[6] Andrey Nikolayevich Tikhonov, Vasiliy Yakovlevich Arsenin, Solution of Ill-Posed Problems, Winston, 1977.
[7] Germana Landi, Elena Loli Piccolomini, An improved newton projection method for nonnegative deblurring of Poisson-corrupted images with tikhonov regularization, Numer. Algorithms 60 (1) (2012) 169–188.
[8] Leonid I. Rudin, Stanley Osher, Emad Fatemi, Nonlinear total variation based noise removal algorithms, Physica D 60 (1) (1992) 259–268.
[9] Germana Landi, Elena Loli Piccolomini, Nptool: a matlab software for nonnegative image restoration with newton projection methods, Numer. Algorithms 62 (3) (2013) 487–504.
[10] Tony Chan, Antonio Marquina, Pep Mulet, High-order total variation-based image restoration, SIAM J. Sci. Comput. 22 (2) (2000) 503–516.
[11] Le Jiang, Jin Huang, Xiao-Guang Lv, Jun Liu, Alternating direction method for the high-order total variation-based Poisson noise removal problem, Numer. Algorithms (2014) 1–22.
[12] Stamatios Lefkimmiatis, Aurélien Bourquard, Michael Unser, Hessian-based norm regularization for image restoration with biomedical applications, IEEE Trans. Image Process. 21 (3) (2012) 983–995.
[13] Jun Liu, Ting-Zhu Huang, Ivan W Selesnick, Xiao-Guang Lv, Po-Yu Chen, Image restoration using total variation with overlapping group sparsity, Inform. Sci. 295 (2015) 232–246.
[14] Fang Li, Chaomin Shen, Jingsong Fan, Chunli Shen, Image restoration combining a total variational filter and a fourth-order filter, J. Vis. Commun. Image Represent. 18 (4) (2007) 322–330.
[15] Konstantinos Papafitsoros, Carola-Bibiane Schönlieb, A combined first and second order variational approach for image reconstruction, J. Math. Imaging Vis. 48 (2) (2014) 308–338.
[16] Jian-Feng Cai, Bin Dong, Stanley Osher, Zuowei Shen, Image restoration: Total variation, wavelet frames, and beyond, J. Amer. Math. Soc. 25 (4) (2012) 1033–1089.
[17] Xue Zhang, Likun Hou, Bin Dong, Zuowei Shen, Xiaoqun Zhang, Proximal iterative hard thresholding methods for wavelet frame based image restoration, Comput. Appl. Math. Rep. 14–85.
[18] Jian-Feng Cai, Stanley Osher, Zuowei Shen, Split bregman methods and frame based image restoration, Multiscale Model. Simul. 8 (2) (2009) 337–369.
[19] You-Wei Wen, Michael K. Ng, Wai-Ki Ching, Iterative algorithms based on decoupling of deblurring and denoising for image restoration, SIAM J. Sci. Comput. 30 (5) (2008) 2655–2674.
[20] Jian-Feng Cai, Stanley Osher, Zuowei Shen, Linearized bregman iterations for frame-based image deblurring, SIAM J. Imaging Sci. 2 (1) (2009) 226–252.
[21] Jian-Feng Cai, Raymond H. Chan, Zuowei Shen, A framelet-based image inpainting algorithm, Appl. Comput. Harmon. Anal. 24 (2) (2008) 131–149.
[22] Mila Nikolova, Michael K. Ng, Shuqin Zhang, Wai-Ki Ching, Efficient reconstruction of piecewise constant images using nonsmooth nonconvex minimization, SIAM J. Imaging Sci. 1 (1) (2008) 2–25.
[23] Mila Nikolova, Michael K. Ng, Chi-Pan Tam, Fast nonconvex nonsmooth minimization methods for image restoration and reconstruction, IEEE Trans. Image Process. 19 (12) (2010) 3073–3088.
[24] Ivan W. Selesnick, Ankit Parekh, Ilker Bayram, Convex 1-D total variation denoising with non-convex regularization, IEEE Signal Process. Lett. 22 (2) (2015) 141–144.
[25] Rick Chartrand, Nonconvex splitting for regularized low-rank+ sparse decomposition, IEEE Trans. Signal Process. 60 (11) (2012) 5810–5819.
[26] Joseph Woodworth, Rick Chartrand, Compressed sensing recovery via nonconvex shrinkage penalties, 2015. arXiv preprint arXiv:1504.02923.
[27] Yin Ding, Ivan W. Selesnick, Artifact-free wavelet denoising: Non-convex sparse regularization, convex optimization, IEEE Signal Process. Lett. 22 (9) (2015) 1364–1368.
[28] Yilun Wang, Junfeng Yang, Wotao Yin, Yin Zhang, A new alternating minimization algorithm for total variation image reconstruction, SIAM J. Imaging Sci. 1 (3) (2008) 248–272.
[29] Raymond H. Chan, Michael K. Ng, Conjugate gradient methods for toeplitz systems, SIAM Rev. 38 (3) (1996) 427–482.
[30] Jinjun Xu, Stanley Osher, Iterative regularization and nonlinear inverse scale space applied to wavelet-based denoising, IEEE Trans. Image Process. 16 (2) (2007) 534–544.
[31] Jean-Baptiste Hiriart-Urruty, Claude Lemaréchal, Fundamentals of Convex Analysis, Springer Science & Business Media, 2001.
[32] Magnus R. Hestenes, Multiplier and gradient methods, J. Optim. Theory Appl. 4 (5) (1969) 303–320.
[33] Stephen Boyd, Lieven Vandenberghe, Convex Optimization, Cambridge University Press, 2004.
[34] Bingsheng He, Hai Yang, Some convergence properties of a method of multipliers for linearly constrained monotone variational inequalities, Oper. Res. Lett. 23 (3) (1998) 151–161.
[35] Chunlin Wu, Xue-Cheng Tai, et al., Augmented lagrangian method, dual methods, and split bregman iteration for rof, vectorial tv, and high order models, SIAM J. Imaging Sci. 3 (3) (2010) 300–339.
[36] Michael K. Ng, Raymond H. Chan, Wun-Cheung Tang, A fast algorithm for deblurring models with Neumann boundary conditions, SIAM J. Sci. Comput. 21 (3) (1999) 851–866.
[37] Jonathan Eckstein, Dimitri P. Bertsekas, On the Douglas–Rachford splitting method and the proximal point algorithm for maximal monotone operators, Math. Program. 55 (1–3) (1992) 293–318.
[38] Bingsheng He, Min Tao, Xiaoming Yuan, Alternating direction method with gaussian back substitution for separable convex programming, SIAM J. Optim. 22 (2) (2012) 313–340.
[39] José M Bioucas-Dias, Mário A.T. Figueiredo, Multiplicative noise removal using variable splitting and constrained optimization, IEEE Trans. Image Process. 19 (7) (2010) 1720–1730.
[40] Stephen Boyd, Neal Parikh, Eric Chu, Borja Peleato, Jonathan Eckstein, Distributed optimization and statistical learning via the alternating direction method of multipliers, Found. Trends Mach. Learn. 3 (1) (2011) 1–122.
[41] Xue-Cheng Tai, Chunlin Wu, Augmented lagrangian method, dual methods and split bregman iteration for rof model, in: Scale Space and Variational Methods in Computer Vision, Springer, 2009, pp. 502–513.
[42] Zhou Wang, Alan C. Bovik, Hamid R. Sheikh, Eero P Simoncelli, Image quality assessment: from error visibility to structural similarity, IEEE Trans. Image Process. 13 (4) (2004) 600–612.
[43] Mário A.T. Figueiredo, José M. Bioucas-Dias, Restoration of Poissonian images using alternating direction optimization, IEEE Trans. Image Process. 19 (12) (2010) 3133–3145.
[44] Yumei Huang, Michael K. Ng, You-Wei Wen, A fast total variation minimization method for image restoration, Multiscale Model. Simul. 7 (2) (2008) 774–795.
[45] James G. Nagy, Katrina Palmer, Lisa Perrone, Iterative methods for image deblurring: a matlab object-oriented approach, Numer. Algorithms 36 (1) (2004) 73–93.
[46] Fang Li, Tieyong Zeng, Image restoration via tight frame regularization and local constraints, J. Sci. Comput. 57 (2) (2013) 349–371.